Chemical Science

RSC Publishing

EDGE ARTICLE

View Article Online
View Journal | View Issue

Cite this: *Chem. Sci.*, 2013, **4**, 1451

Submillisecond-lived photoinduced charge separation in inclusion complexes composed of $Li^+@C_{60}$ and cyclic porphyrin dimers†

Takuya Kamimura,[a] Kei Ohkubo,[b] Yuki Kawashima,[b] Hirofumi Nobukuni,[a] Yoshinori Naruta,[a] Fumito Tani*[a] and Shunichi Fukuzumi*[bc]

Received 24th November 2012
Accepted 7th January 2013

DOI: 10.1039/c3sc22065f

www.rsc.org/chemicalscience

Lithium ion encapsulated [60]fullerene ($Li^+@C_{60}$) is included within a free base and nickel complex of a cyclic porphyrin dimer (M-CPD_{Py}, M = H_4 and Ni_2) to afford supramolecules ($Li^+@C_{60}\subset$M-CPD_{Py}) in a polar solvent (benzonitrile) with the association constants of 2.6×10^5 M^{-1} and 3.5×10^5 M^{-1}, respectively. From the electrochemical analysis, the energies of the charge-separated (CS) states are estimated to be 1.07 eV for $Li^+@C_{60}\subset H_4$-CPD_{Py} and 1.20 eV for $Li^+@C_{60}\subset Ni_2$-CPD_{Py}. Both values are lower than the triplet excited energies of the fullerene and porphyrin. Upon the photoexcitation at the Q-band of the porphyrin chromophore of $Li^+@C_{60}\subset H_4$-CPD_{Py}, electron transfer from the triplet excited state of the free base porphyrin to $Li^+@C_{60}$ occurs to produce the CS state. $Li^+@C_{60}\subset Ni_2$-CPD_{Py} also undergoes photoinduced electron transfer to produce the CS state. The lifetimes of the resulting CS states are 0.50 ms for $Li^+@C_{60}\subset H_4$-CPD_{Py} and 0.67 ms for $Li^+@C_{60}\subset Ni_2$-CPD_{Py}. These remarkably long CS lifetimes are the best values ever reported for non-covalent porphyrin-fullerene supramolecules in solution and are attributable to the lower CS energies than the triplet energy of each chromophore.

Introduction

In a natural photosynthetic reaction centre, the multistep electron-transfer reactions occur following the excitation of dimeric chlorophyll to attain the long-lived charge-separated (CS) state.[1] The redox-active components such as chlorophyll, pheophytin and quinones are elegantly located in the protein matrix by non-covalent interactions.[1] Extensive efforts have so far been devoted toward the design of electron donor–acceptor composites using covalently and non-covalently linked systems to form the long-lived CS state upon photoexcitation.[2–26] The syntheses of covalently linked systems are inefficient and costly, thus it is a better choice to prepare supramolecular donor and acceptor systems.[13–21]

Fullerenes and porphyrins are attractive building blocks for the construction of supramolecular electron donor–acceptor composites due to their excellent photophysical and electron-transfer properties.[13–26] The fullerene derivatives have been widely employed as electron acceptors due to their favourable reduction potentials and small reorganization energy in electron-transfer reactions.[20–28] On the other hand, the porphyrin compounds have very strong absorption bands in the visible region and their photoexcited states are generally good electron donors.[28] Moreover, porphyrins are attractive components in the construction of host molecules for fullerenes through the π–π interactions between the spherical π-surface of fullerenes and flat π-planes of porphyrins.[29–36] Numerous fullerene-porphyrin supramolecules as well as linked molecules have been extensively studied as functional models of the reaction centre for charge-separation process in natural photosynthesis.[12–21,30–35] However, non-covalent binding between highly π-conjugated compounds such as porphyrins and fullerenes is not strong enough in polar solvents which are generally used for studies on photoinduced electron-transfer reactions. In contrast, when a non-polar solvent is used, the efficiency of charge separation is low in the supramolecular donor–acceptor complexes and the resulting CS state is extremely short-lived because the CS state decays to the triplet excited chromophore, which is lower in energy than the CS state.[12,24b] The energy of CS state should be lower than the triplet excited energy of each component. This is a typical dilemma for the long-lived charge separation in supramolecular donor–acceptor complexes.

In order to solve this problem, we have recently reported the cyclic porphyrin dimers (CPDs) as shown in Scheme 1a.[35] Receptor molecules composed of multiple porphyrins are suitable for the inclusion of pristine C_{60} and the derivatives. The

[a]*Institute for Materials Chemistry and Engineering, Kyushu University, Fukuoka 812-8581, Japan. E-mail: tanif@ms.ifoc.kyushu-u.ac.jp; Fax: +81-92-642-2732; Tel: +81-92-642-2732*

[b]*Department of Material and Life Science, Graduate School of Engineering, Osaka University, ALCA, Japan Science and Technology (JST), Suita, Osaka 565-0871, Japan. E-mail: fukuzumi@chem.eng.osaka-u.ac.jp; Fax: +81-6-6879-7370; Tel: +81-6-6879-7368*

[c]*Department of Bioinspired Science, Ewha Womans University, Seoul, 120–750, Korea*

† Electronic supplementary information (ESI) available: Spectroscopic and kinetic data. See DOI: 10.1039/c3sc22065f

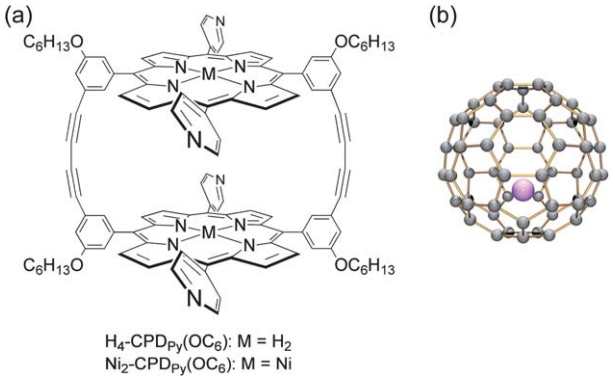

Scheme 1 Structures of (a) $CPD_{Py}(OC_6)$ and (b) $Li^+@C_{60}$.

strong supramolecular binding by π–π interaction was observed to form inclusion complexes.[35,36] Unfortunately, the inclusion complex of C_{60} and the nickel cyclic porphyrin dimer ($C_{60}\subset Ni_2$-CPD_{Py}) in crystalline state did not show the expected CS state in the time-resolved transient absorption spectra upon photoexcitation because the singlet excited state of the nickel porphyrin immediately gives rise to the triplet excited state by the rapid intersystem crossing, followed by energy transfer to afford the low-energy triplet excited state of C_{60} ($^3C_{60}^*$).[35] The estimated energy level of the CS state (1.98 eV) is higher than that of $^3C_{60}^*$ (1.57 eV).[35,37] In contrast, the corresponding inclusion complex of C_{60} and the free-base porphyrin dimer ($C_{60}\subset H_4$-CPD_{Py}) underwent photoinduced electron transfer from the porphyrin to C_{60} owing to the lower oxidation potential and the slower intersystem crossing of the free-base porphyrin than those of the nickel complex. However, the lifetime of this CS state was very short probably because its energy level (1.83 eV) is still higher than that of $^3C_{60}^*$.[35] The energy limit of a CS state is *ca.* 1.50–1.60 eV, which is the triplet excited energies of fullerenes and porphyrins.[19]

It has been reported that a lithium ion encapsulated fullerene ($Li^+@C_{60}$) has a stronger electron accepting ability than pristine C_{60}.[38–42] The higher reduction potential of $Li^+@C_{60}$ than C_{60} makes the energy levels of the resulting CS states lower than the triplet excited energy.[40,41] It is expected that the combination of $Li^+@C_{60}$ and the cyclic porphyrin dimers will make it possible to achieve both efficient formation of supramolecules and long-lived photoinduced charge separation. Thus, we report herein that supramolecular systems composed of cyclic porphyrin dimers and $Li^+@C_{60}$ afford photoinduced CS states with higher energies and longer lifetimes than those composed of $Li^+@C_{60}$ and monomeric porphyrins.[41]

Results and discussion

1 Supramolecular formation of cyclic porphyrin dimers with $Li^+@C_{60}$

Cyclic porphyrin dimers without OC_6H_{13} groups have poor solubility in organic solvents.[35,36] Therefore, we have designed and prepared new dimers with four long alkoxy substituents on the *meso*-phenyl groups (H_4–, Ni_2–$CPD_{Py}(OC_6)$, Scheme 1) to improve the solubility. The synthetic procedures are shown in Scheme 2. The products were characterized by ^{1}H-NMR, ^{13}C-NMR, IR and mass spectroscopies (see the Experimental section and ESI† S1–S14). They are sufficiently soluble in benzonitrile (PhCN) to allow photochemical and electrochemical analysis with $Li^+@C_{60}$ in solution.

UV-vis absorption spectral changes were observed by addition of $Li^+@C_{60}$ PF_6^- to PhCN solutions of H_4-$CPD_{Py}(OC_6)$ and Ni_2-$CPD_{Py}(OC_6)$ as shown in Fig. 1 and Fig. S15 in ESI,† respectively. The Soret absorption bands of H_4-$CPD_{Py}(OC_6)$ and Ni_2-$CPD_{Py}(OC_6)$ were red-shifted and decreased in intensity with isosbestic points at 428 nm. The Job's plots upon mixing of $Li^+@C_{60}$ with H_4-$CPD_{Py}(OC_6)$ and Ni_2-$CPD_{Py}(OC_6)$ displayed typical signature patterns for the formation of a 1 : 1 host–guest complex ($Li^+@C_{60}\subset H_4$-$CPD_{Py}(OC_6)$ and $Li^+@C_{60}\subset Ni_2$-$CPD_{Py}(OC_6)$, see Fig. S16 in ESI†). On the basis of the titration of H_4-$CPD_{Py}(OC_6)$ and Ni_2-$CPD_{Py}(OC_6)$ with $Li^+@C_{60}$ at 298 K, the association constants (K_{assoc}) were determined to be 2.6×10^5 M^{-1} for $Li^+@C_{60}\subset H_4$-$CPD_{Py}(OC_6)$ and 3.5×10^5 M^{-1} for $Li^+@C_{60}\subset Ni_2$-$CPD_{Py}(OC_6)$ by applying a nonlinear curve-fitting method using eqn (1) and (2),

$$\Delta Abs = L\{1 + K_{assoc}A + K_{assoc}X - [(1 + K_{assoc}A + K_{assoc}X)^2 - 4K_{assoc}{}^2AX]^{0.5}\}/2K_{assoc}A \quad (1)$$

$$\Delta Int = F\{1 + K_{assoc}A + K_{assoc}X - [(1 + K_{assoc}A + K_{assoc}X)^2 - 4K_{assoc}{}^2AX]^{0.5}\}/2K_{assoc}A \quad (2)$$

where A and X are $[Host]_0$ and $[Guest]_0$, respectively; L and F are ΔAbs and ΔInt at 100% complexation, respectively. L, F and K_{assoc} were treated as fitting parameters. The K_{assoc} values thus determined are slightly higher than those of pristine C_{60} (1.9×10^5 M^{-1} for $C_{60}\subset H_4$-$CPD_{Py}(OC_6)$ and 2.5×10^5 M^{-1} for $C_{60}\subset Ni_2$-$CPD_{Py}(OC_6)$) (Fig. S17 in ESI†). The data are summarized in Table 1.

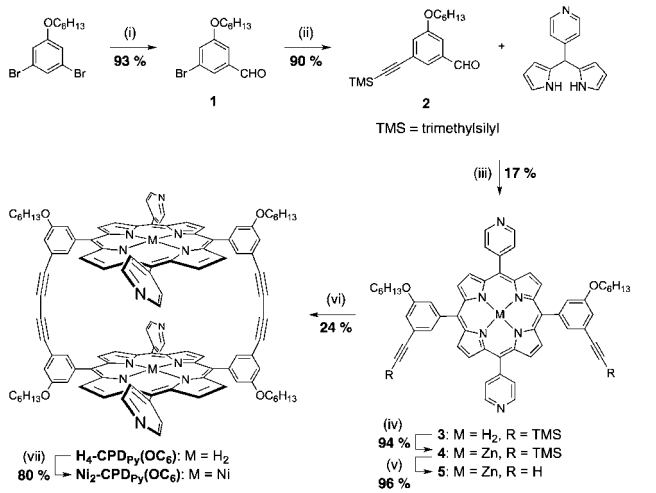

Scheme 2 Synthetic pathway for H_4–$CPD_{Py}(OC_6)$ and Ni_2–$CPD_{Py}(OC_6)$. (i) *n*-Butyllithium, DMF, THF; (ii) trimethylsilylacetylene, $Pd(OAc)_2$, Ph_3P, Et_3N; (iii) TFA, DDQ, CH_2Cl_2; (iv) $Zn(OAc)_2$, CH_2Cl_2; (v) KF·$2H_2O$, DMF/THF; (vi) CuCl, pyridine, air and (vii) $Ni(OAc)_2\cdot 4H_2O$, $CHCl_3$/toluene (3/2 v/v).

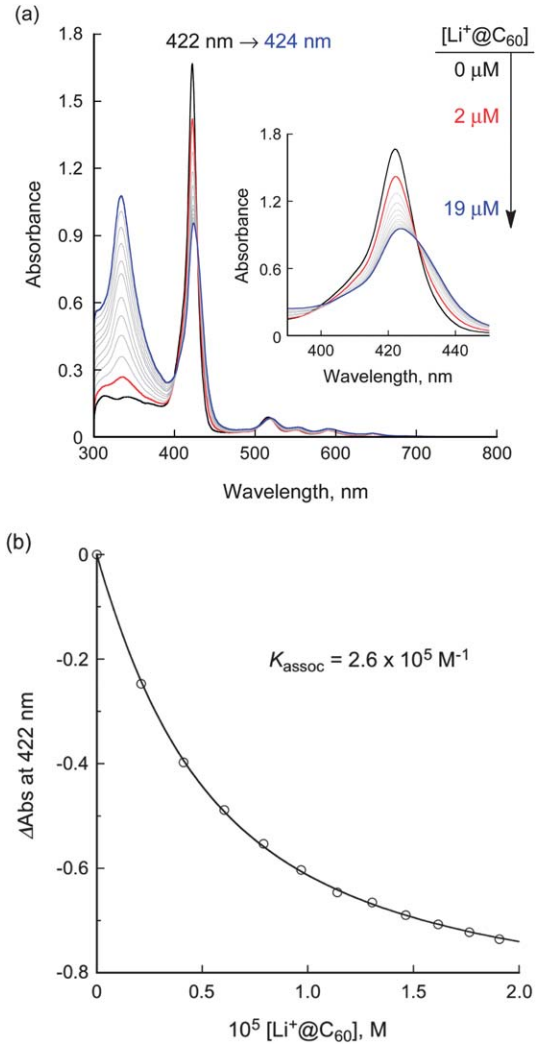

Fig. 1 (a) UV-vis absorption changes of H_4-$CPD_{Py}(OC_6)$ in the course of titration with $Li^+@C_{60}$ in PhCN at room temperature. $[H_4\text{-}CPD_{Py}(OC_6)] = 2.5 \times 10^{-6}$ M. The inset shows the Soret band region. (b) Changes in the UV-vis absorbance (ΔAbs) at 422 nm. The curve was fitted by using eqn (1).

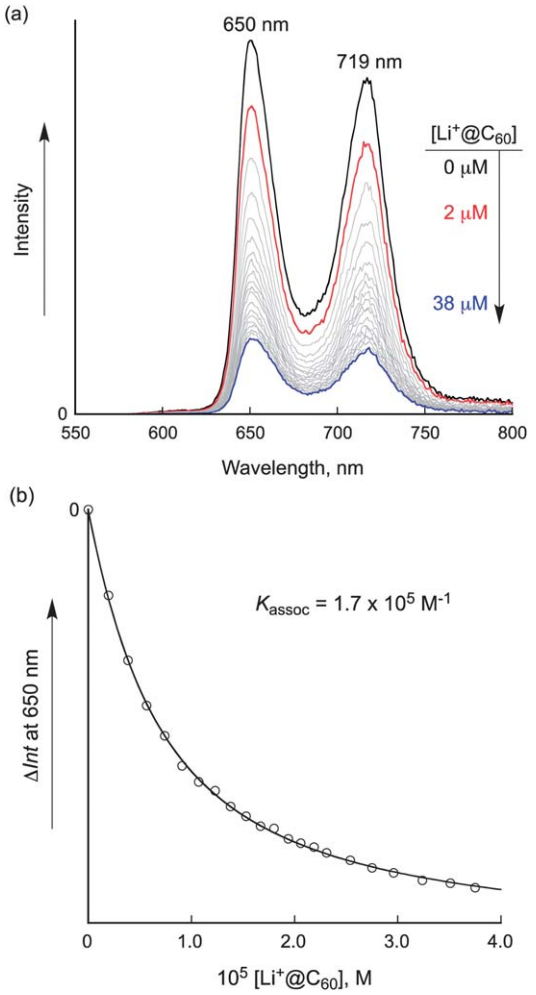

Fig. 2 (a) Fluorescence spectral changes of H_4–$CPD_{Py}(OC_6)$ in the course of titration with $Li^+@C_{60}$ in deaerated PhCN at 298 K excited at 430 nm. $[H_4\text{–}CPD_{Py}(OC_6)] = 2.5 \times 10^{-6}$ M. (b) Changes in the fluorescence intensity (ΔInt) at 650 nm. The K_{assoc} value was evaluated by using eqn (2).

Upon photoexcitation at the Soret band (430 nm) of H_4–$CPD_{Py}(OC_6)$ in PhCN, the fluorescence due to the porphyrin is observed at $\lambda_{max} = 650$ and 717 nm as shown in Fig. 2. Addition of $Li^+@C_{60}$ to a PhCN solution of H_4-$CPD_{Py}(OC_6)$ induced a noticeable decrease in the fluorescence intensity of H_4-$CPD_{Py}(OC_6)$. From the plot of the fluorescence intensity change *vs.* the concentration of $Li^+@C_{60}$, the K_{assoc} value was determined to be 1.7×10^5 M^{-1}, which agrees with the value obtained from the absorption spectral change within an experimental error (*vide supra*).

Table 1 The association constants, rate constant of electron transfer, CS lifetimes and quantum yields of H_4-$CPD_{Py}(OC_6)$ and Ni_2-$CPD_{Py}(OC_6)$ in deaerated PhCN at 298 K

	K_{assoc},[a] M^{-1}	K_{assoc},[b] M^{-1}	k_{ET}, s^{-1}	τ(CS), ms	Φ(CS)
$H_4CPD_{Py}(OC_6)$	2.6×10^5	1.7×10^5	—	0.50	0.32
$Ni_2CPD_{Py}(OC_6)$	3.5×10^5	[c]	5.7×10^7	0.67	0.13

[a] Determined from the absorption change. [b] Determined from the fluorescence change. [c] No emission from $Ni_2CPD_{Py}(OC_6)$.

2 Energetics of photoinduced processes

Cyclic voltammograms of $Li^+@C_{60}\subset H_4$–$CPD_{Py}(OC_6)$ and $Li^+@C_{60}\subset Ni_2$–$CPD_{Py}(OC_6)$ are shown in Fig. 3a and b. The comparison with the uncomplexed compounds shows that the cyclic voltammograms consist of the electron oxidation processes of $CPD_{Py}(OC_6)$ and the electron reduction process of $Li^+@C_{60}$.[43] The electrochemical data are summarized in Table 2. The energy of the CS states determined from the potential difference between one-electron reduction and oxidation potentials are 1.07 eV for $Li^+@C_{60}\subset H_4$–$CPD_{Py}(OC_6)$ and 1.20 eV for $Li^+@C_{60}\subset Ni_2$–$CPD_{Py}(OC_6)$. These values are smaller than those of the singlet excited states of cyclic porphyrin dimers (1.90 eV for H_4–$CPD_{Py}(OC_6)$,[35c] 1.97 eV for Ni_2–$CPD_{Py}(OC_6)$,[35b] and 1.94 eV for $Li^+@C_{60}$ (ref. 40)). Thus, the free energy changes of photoinduced electron transfer to $Li^+@C_{60}$ *via* the singlet excited states are negative (exergonic).

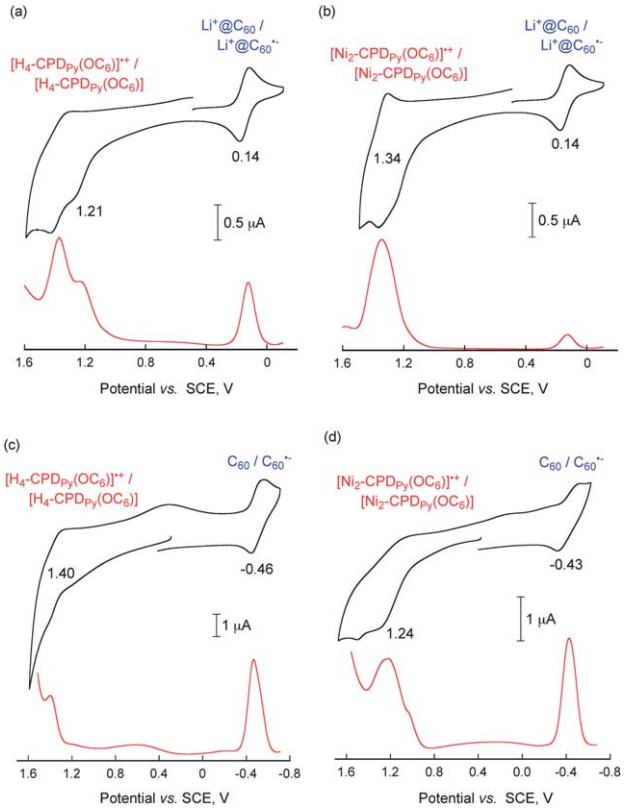

Fig. 3 Cyclic voltammograms (CV) and differential pulse voltammograms (DPV) of (a) $Li^+@C_{60}\subset H_4$–$CPD_{Py}(OC_6)$, (b) $Li^+@C_{60}\subset Ni_2$–$CPD_{Py}(OC_6)$, (c) $C_{60}\subset H_4$–$CPD_{Py}(OC_6)$, and (d) $C_{60}\subset Ni_2$–$CPD_{Py}(OC_6)$ in deaerated PhCN containing 0.10 M $TBAPF_6$. (a and b) $[CPD_{Py}(OC_6)] = [Li^+@C_{60}] = 2.5 \times 10^{-4}$ M, (c and d) $[CPD_{Py}(OC_6)] = [C_{60}] = 2.0 \times 10^{-4}$ M. Conditions: (a, b and d) 100 mV s^{-1} and (c) 500 mV s^{-1} for CV, and 4 mV s^{-1} for DPV.

Table 2 Redox potentials (*V vs.* SCE) and CS energies (eV) of $Li^+@C_{60}\subset CPD_{Py}(OC_6)$ and $C_{60}\subset CPD_{Py}(OC_6)$ in PhCN containing 0.10 M $TBAPF_6$

Compound	Reduction $E^{1/2}$, V	Oxidation $E^{1/2}$, V	CS energy, eV
$Li^+@C_{60}\subset H_4$–$CPD_{Py}(OC_6)$	0.14	1.21	1.07
$Li^+@C_{60}\subset Ni_2$–$CPD_{Py}(OC_6)$	0.14	1.34	1.20
$C_{60}\subset H_4$–$CPD_{Py}(OC_6)$	−0.46	1.40	1.86
$C_{60}\subset Ni_2$–$CPD_{Py}(OC_6)$	−0.43	1.24	1.67

The energies of the triplet excited states were determined by phosphorescence spectra in a frozen PrCN/EtI (3:1 v/v) glasses at 77 K to be 1.51 eV for H_4–$CPD_{Py}(OC_6)$ and 1.50 eV for Ni_2–$CPD_{Py}(OC_6)$ (Fig. S18 in ESI†). The energy of the triplet excited state of $Li^+@C_{60}$ ($^3[Li^+@C_{60}]^*$; * denotes the excited state) was reported to be 1.53 eV.[39,40] The energy level of the resulting CS states are lower than those of the triplet excited states of both $Li^+@C_{60}$ and the porphyrin dimers. Thus, photoinduced electron transfer from the singlet or triplet excited state of the porphyrin dimers to $Li^+@C_{60}$ as well as from the porphyrin dimers to the singlet or triplet excited state of $Li^+@C_{60}$ is energetically possible in the supramolecular complexes to form the CS states.

In contrast to the case of $Li^+@C_{60}$, the estimated energy levels of the CS states of $C_{60}\subset H_4$-$CPD_{Py}(OC_6)$ and $C_{60}\subset Ni_2$-$CPD_{Py}(OC_6)$ and (1.86 and 1.67 eV) are higher than those of the triplet excited state of C_{60} and $CPD_{Py}(OC_6)$ as observed in our previous studies,[35] suggesting no formation or short lifetimes of the CS states.

3 Photoinduced charge separation

The photodynamics of these inclusion complexes was investigated by the transient absorption spectra measured in PhCN by the use of femtosecond and nanosecond laser flash photolysis. The time-resolved transient absorption spectra of $Li^+@C_{60}\subset H_4$–$CPD_{Py}(OC_6)$ measured by femtosecond laser flash photolysis ($\lambda_{ex} = 420$ nm) in the time range from 1 ps to 3000 ps (Fig. 4a), which showed little difference from the transient spectra of only H_4–$CPD_{Py}(OC_6)$ (Fig. S19a in ESI†), showing a characteristic absorption due to the singlet excited state of H_4-$CPD_{Py}(OC_6)$ ($^1[H_4$–$CPD_{Py}(OC_6)]^*$). The decay rate constant of $^1[H_4$–$CPD_{Py}(OC_6)]^*$ to the triplet excited state ($^3[H_4$–$CPD_{Py}(OC_6)]^*$) was determined from the absorption change at 630 nm (inset of Fig. 4a) to be 1.0×10^9 s^{-1}, which is slightly larger than the value of intersystem crossing of $^1[H_4$-$CPD_{Py}(OC_6)]^*$ without $Li^+@C_{60}$ ($k_{ISC} = 8.0 \times 10^8$ s^{-1}) (Fig. S19a in ESI†). No characteristic absorption band due to $Li^+@C_{60}^{\bullet-}$ was observed at $\lambda_{max} = 1035$ nm.[39–41] Thus, no electron transfer from $^1[H_4$–$CPD_{Py}(OC_6)]^*$ or $^3[H_4$–$CPD_{Py}(OC_6)]^*$ to $Li^+@C_{60}$ occurred in the time range of femtosecond laser flash photolysis (~3000 ps).

Similarly, the transient absorption spectra of $Li^+@C_{60}\subset Ni_2$–$CPD_{Py}(OC_6)$ measured by femtosecond transient absorption spectroscopy (Fig. 4b) indicates only the occurrence of the rapid intersystem crossing of $^1[Ni_2$–$CPD_{Py}(OC_6)]^*$ to $^3[Ni_2$–$CPD_{Py}(OC_6)]^*$ ($k_{ISC} > 10^{12}$ s^{-1}), in comparison with the transient spectra of only Ni_2–$CPD_{Py}(OC_6)$ (Fig. S19b in ESI†).[44] The intersystem crossing process was not detected by use of our femtosecond laser system (fwhm = 130 fs). The k_{ISC} value to $^3[Ni_2$–$CPD_{Py}(OC_6)]^*$ is much larger than that to $^3[H_4$–$CPD_{Py}(OC_6)]^*$ because of the heavy atom effect of Ni. $^3[N_2$–$CPD_{Py}(OC_6)]^*$ decayed to the ground state with the rate constant of $k_T = 5.3 \times 10^9$ s^{-1}.

In contrast to the results of femtosecond laser flash photolysis in Fig. 4, where no electron transfer was observed, nanosecond laser excitation of $Li^+@C_{60}\subset H_4$–$CPD_{Py}(OC_6)$ resulted in observation of transient absorption bands at 690 and 1035 nm due to H_4–$CPD_{Py}(OC_6)^{\bullet+}$ and $Li^+@C_{60}^{\bullet-}$, respectively (Fig. 5a).[39–41] This clearly indicates the occurrence of electron transfer from $^3[H_4$–$CPD_{Py}(OC_6)]^*$ to $Li^+@C_{60}$ to produce the CS state ($Li^+@C_{60}^{\bullet-}\subset H_4$–$CPD_{Py}(OC_6)^{\bullet+}$). The rate of electron transfer from $^3[H_4$–$CPD_{Py}(OC_6)]^*$ to $Li^+@C_{60}$ was too fast to detect in the time scale of the nanosecond laser flash photolysis experiments ($k_{ET} > 10^7$ s^{-1}).[45] The absorbance at 1035 nm due to $Li^+@C_{60}^{\bullet-}$ in the CS state decayed obeying first-order kinetics with the same slope irrespective of the difference in the laser intensity. This clearly indicates that the decay of the CS state occurs *via* intrasupramolecular back electron transfer rather than a bimolecular reaction. The CS lifetime was determined from the slope of the first-order plots in Fig. 5b to be 0.50 ms.

Similarly nanosecond laser excitation of $Li^+@C_{60}\subset Ni_2$–$CPD_{Py}(OC_6)$ at 520 nm also results in formation of the CS state ($Li^+@C_{60}^{\bullet-}\subset Ni_2$–$CPD_{Py}(OC_6)^{\bullet+}$) as shown in Fig. 6a, where

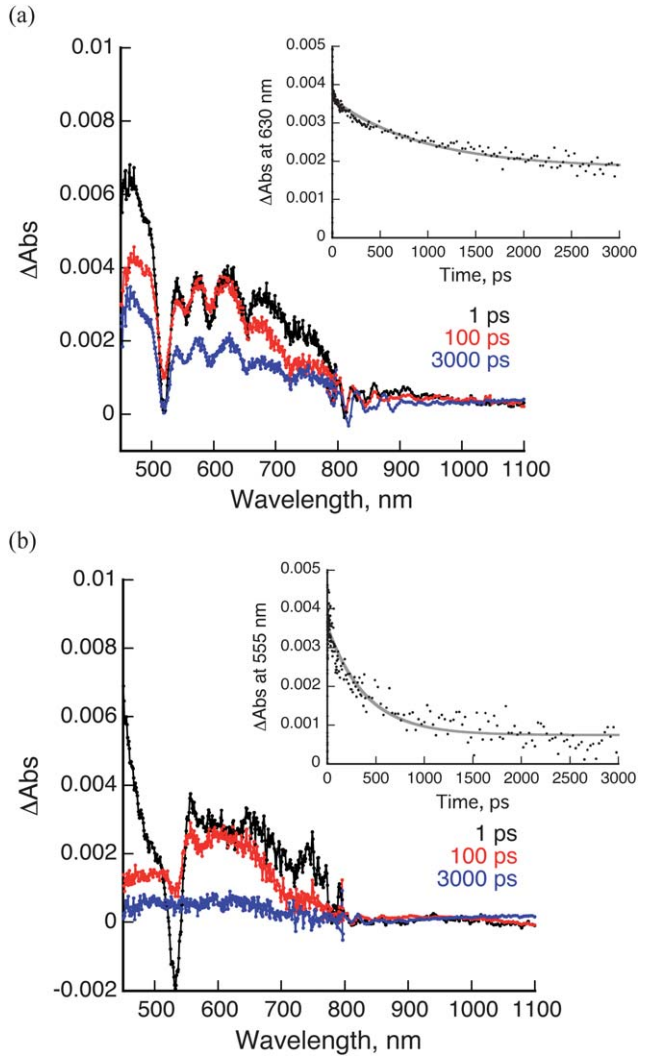

Fig. 4 (a) Transient absorption spectra of H_4–$CPD_{Py}(OC_6)$ with $Li^+@C_{60}$ in deaerated PhCN at room temperature taken at 1, 100, and 3000 ps after femtosecond laser excitation at 420 nm. $[H_4–CPD_{Py}(OC_6)] = 7.0 \times 10^{-6}$ M, $[Li^+@C_{60}] = 1.4 \times 10^{-5}$ M. (b) Transient absorption spectra of Ni_2–$CPD_{Py}(OC_6)$ with $Li^+@C_{60}$ in deaerated PhCN at room temperature taken at 1, 100, and 3000 ps after femtosecond laser excitation at 420 nm. $[Ni_2–CPD_{Py}(OC_6)] = 1.0 \times 10^{-5}$ M, $[Li^+@C_{60}] = 2.0 \times 10^{-5}$ M.

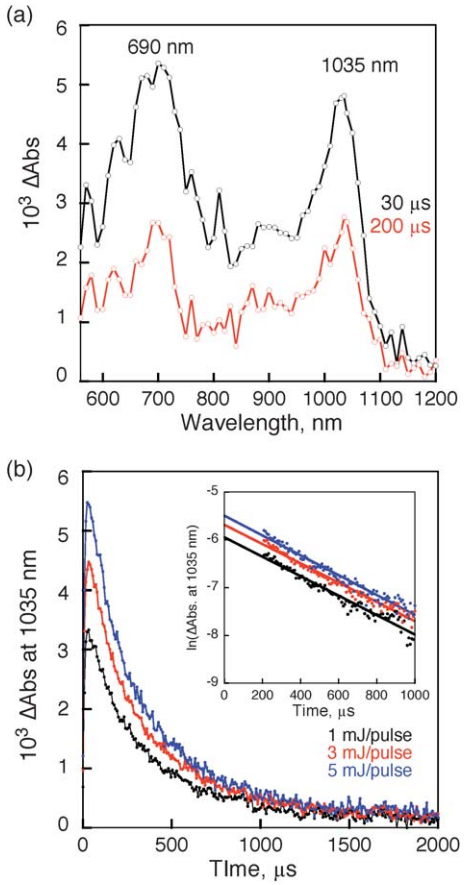

Fig. 5 (a) Transient absorption spectra of H_4–$CPD_{Py}(OC_6)$ with $Li^+@C_{60}$ in deaerated PhCN at room temperature taken at 30 and 200 μs after nanosecond laser excitation at 505 nm. $[H_4–CPD_{Py}(OC_6)] = 2.5 \times 10^{-5}$ M, $[Li^+@C_{60}] = 5.0 \times 10^{-5}$ M. (b) Decay time profiles at 1035 nm with different laser intensities (1, 3, 5 mJ per pulse). Inset: first-order plots.

transient absorption bands due to Ni_2–$CPD_{Py}(OC_6)^+$ and $Li^+@C_{60}^-$ were observed. In this case, however electron transfer occurs from Ni_2–$CPD_{Py}(OC_6)$ to the triplet excited state of $Li^+@C_{60}$ ($^3[Li^+@C_{60}]^*$) rather than from $^3[Ni_2–CPD_{Py}(OC_6)]^*$ to $Li^+@C_{60}$ as indicated by the disappearance of the absorption band at 750 nm due to $^3[Li^+@C_{60}]^*$, accompanied by the appearance of the absorption band at 1035 nm due to $Li^+@C_{60}^-$ (Fig. 6b). Photoexcitation at 520 nm where $Li^+@C_{60}$ has absorption results in the formation of $^1[Li^+@C_{60}]^*$, which is converted to $^3[Li^+@C_{60}]^*$ *via* the intersystem crossing. The rate constant of electron transfer from Ni_2–$CPD_{Py}(OC_6)$ to $^3[Li^+@C_{60}]^*$ to produce the CS state was determined from the rise in the absorbance at 1035 nm due to $Li^+@C_{60}^-$ to be 5.7×10^7 s^{-1}. The CS lifetime was determined from the slope of the first-order plots in Fig. 6c to be 0.67 ms, which is the longest value ever reported for non-covalent porphyrin-fullerene supramolecules in solution.[41,46] The quantum yields of the CS states were estimated to be 0.32 for $Li^+@C_{60}\subset H_4$–$CPD_{Py}(OC_6)$ and 0.13 for $Li^+@C_{60}\subset Ni_2$–$CPD_{Py}(OC_6)$ by means of the comparative method with the absorption intensities of the CS states ($Li^+@C_{60}^-$: $\sum$ (1035 nm) = 7300 M^{-1} cm^{-1}).[23,39]

When $Li^+@C_{60}$ was replaced by pristine C_{60}, the transient absorption spectra of both $C_{60}\subset H_4$–$CPD_{Py}(OC_6)$ and $C_{60}\subset Ni_2$–$CPD_{Py}(OC_6)$ measured by nanosecond laser flash photolysis in PhCN exhibited only 740 nm bands for the triplet excited state of C_{60} with no transient absorption bands due to $CPD_{Py}(OC_6)^+$ or C_{60}^- (Fig. S20 in ESI†). Thus, no CS states were produced as predicted by their higher energy levels than those of the triplet excited states of $CPD_{Py}(OC_6)$ and C_{60}.

The temperature dependence of the charge recombination (CR) process was investigated by nanosecond laser flash photolysis in the range of 25–70 °C for $Li^+@C_{60}\subset H_4$–$CPD_{Py}(OC_6)$ and 25–80 °C for $Li^+@C_{60}\subset Ni_2$–$CPD_{Py}(OC_6)$. The activation enthalpies were determined from the Eyring plots of the rate constants (k_{BET}) of the back electron transfer (charge recombination) to be 3.5 kcal mol^{-1} for both $Li^+@C_{60}\subset H_4$–$CPD_{Py}(OC_6)$ and $Li^+@C_{60}\subset Ni_2$–$CPD_{Py}(OC_6)$ (Fig. S21 in ESI†).

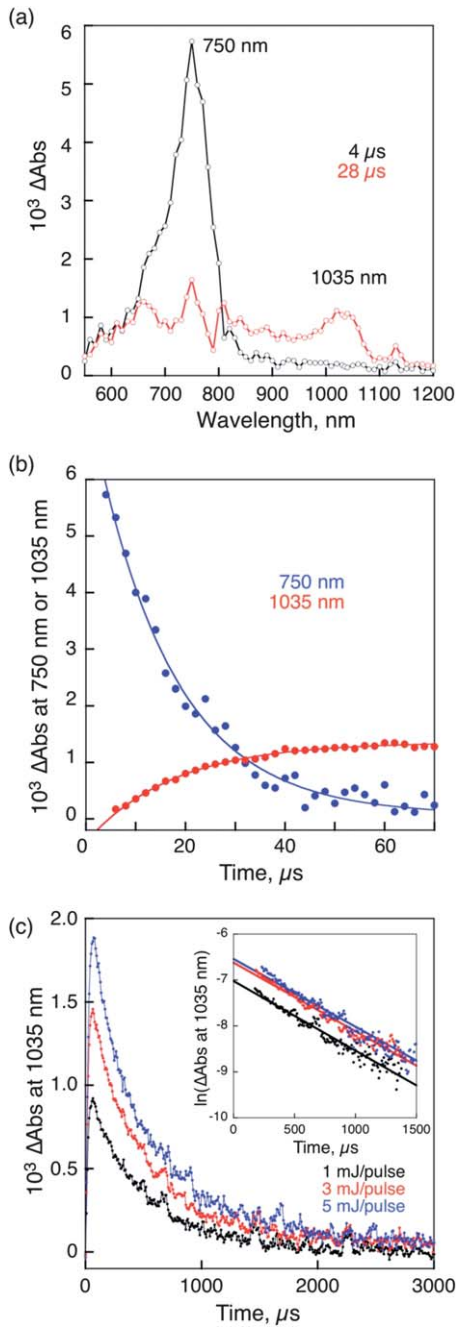

Fig. 6 (a) Transient absorption spectra of Ni_2–$CPD_{Py}(OC_6)$ with $Li^+@C_{60}$ in deaerated PhCN at room temperature taken at 4 and 28 μs after nanosecond laser excitation at 520 nm. $[Ni_2–CPD_{Py}(OC_6)] = 2.5 \times 10^{-5}$ M, $[Li^+@C_{60}] = 5.0 \times 10^{-5}$ M. (b) Rise and (c) decay time profiles at 1035 nm with different laser intensities (1, 3, 5 mJ per pulse). Inset: first-order plots.

The linear plots of $\ln(k_{BET}\,T^{1/2})$ *vs.* T^{-1} derived from the Marcus equation (eqn (3))[47] in Fig. 7 afford the reorganization

$$\ln\left(k_{BET}T^{1/2}\right) = \ln\left(\frac{2\pi^{3/2}V^2}{h(\lambda k_B)^{1/2}}\right) - \frac{(\Delta G_{BET} + \lambda)^2}{4\lambda k_B T} \qquad (3)$$

energies (λ) and electronic coupling matrix elements (V) for the BET: $\lambda = 0.56$ eV and $V = 0.11$ cm^{-1} for $Li^+@C_{60}$⊂H_4–$CPD_{Py}(OC_6)$, $\lambda = 0.54$ eV and $V = 0.10$ cm^{-1} for $Li^+@C_{60}$⊂Ni_2–$CPD_{Py}(OC_6)$. The appreciable temperature dependence of k_{BET} indicates that the BET process is deeply in the Marcus inverted region, where the k_{BET} value decreases with increasing the driving force.[47]

Based on the results described above, the mechanisms of intrasupramolecular photoinduced charge separation in $Li^+@C_{60}$⊂H_4–$CPD_{Py}(OC_6)$ and $Li^+@C_{60}$⊂Ni_2–$CPD_{Py}(OC_6)$ are proposed as shown in Schemes 3 and 4, respectively. The singlet excited state of H_4–$CPD_{Py}(OC_6)$ ($^1[H_4–CPD_{Py}(OC_6)]^*$) is generated upon photoexcitation of $Li^+@C_{60}$⊂H_4–$CPD_{Py}(OC_6)$ at 420 nm, where the porphyrin moiety is exclusively excited. Even if the $Li^+@C_{60}$ moiety is excited, energy transfer from $^1[Li^+@C_{60}]^*$ (E_s = 1.94 eV) to H_4–$CPD_{Py}(OC_6)$ (E_s = 1.90 eV) may occur to produce $^1[H_4–CPD_{Py}(OC_6)]^*$. Although electron transfer from $^1[H_4–CPD_{Py}(OC_6)]^*$ to $Li^+@C_{60}$ energetically possible (Scheme 3), the intersystem crossing to generate $^3[H_4–CPD_{Py}(OC_6)]^*$ occurs with the rate constant of 8.3×10^8 s^{-1}. Then, electron transfer occurs from $^3[H_4–CPD_{Py}(OC_6)]^*$ to $Li^+@C_{60}$ with the driving force of 0.44 eV to produce the CS state with a much larger rate constant ($k_{ET} > 10^7$ s^{-1}) than the triplet decay to the ground state ($k_T = 2.1 \times 10^3$ s^{-1}). The CS state decays slowly *via* intrasupramolecular BET with the lifetime of 0.50 ms (Scheme 3).

As the case of $Li^+@C_{60}$⊂Ni_2–$CPD_{Py}(OC_6)$, photoexcitation of $Li^+@C_{60}$⊂Ni_2–$CPD_{Py}(OC_6)$ at 420 nm, where the porphyrin moiety is excited exclusively, results in formation of the singlet excited state ($^1[Ni_2–CPD_{Py}(OC_6)]^*$) as shown in Scheme 4. In contrast to the case of H_4–$CPD_{Py}(OC_6)$, however, the intersystem crossing to $^3[Ni_2–CPD_{Py}(OC_6)]^*$ occurs rapidly with the rate constant ($k_{ISC} > 10^{12}$ s^{-1}). $^3[Ni_2–CPD_{Py}(OC_6)]^*$ decays to the ground state prior to electron transfer from $^3[Ni_2–CPD_{Py}(OC_6)]^*$ to $Li^+@C_{60}$.[48] Photoexcitation of $Li^+@C_{60}$⊂Ni_2–$CPD_{Py}(OC_6)$ at 520 nm, where $Li^+@C_{60}$ has absorption, generates the singlet excited state ($^1[Li^+@C_{60}]^*$). After the intersystem crossing, electron transfer from Ni_2–$CPD_{Py}(OC_6)$ to $^3[Li^+@C_{60}]^*$ occurs with the rate constant of 5.7×10^7 s^{-1} to produce the CS state. The CS state decays slowly with the lifetime of 0.67 ms (Scheme 4).

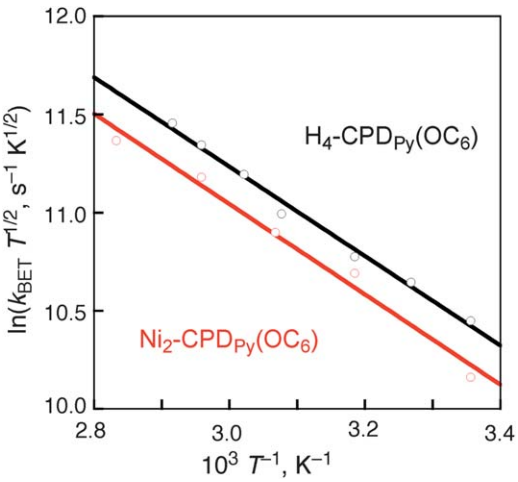

Fig. 7 Plots of $\ln(k_{BET}\,T^{1/2})$ *vs.* T^{-1} for charge recombination of $[H_4–CPD_{Py}(OC_6)^{+}$ + $Li^+@C_{60}^{\cdot-}]$ (black) and $[Ni_2–CPD_{Py}(OC_6)^{+}$ + $Li^+@C_{60}^{\cdot-}]$ (red) in PhCN.

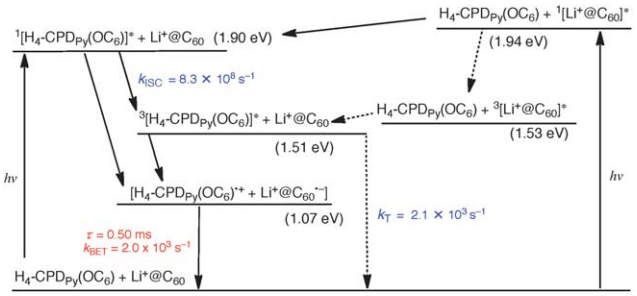

Scheme 3 Energy diagram for $Li^+@C_{60}\subset H_4$–$CPD_{Py}(OC_6)$; broken arrow: minor pathway.

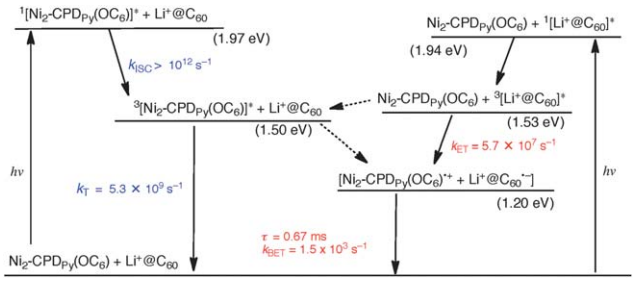

Scheme 4 Energy diagram for $Li^+@C_{60}\subset Ni_2$–$CPD_{Py}(OC_6)$; broken arrow: minor pathway.

Conclusions

$Li^+@C_{60}$ is included within a free base and nickel complex of a cyclic porphyrin dimer to give stable supramolecules in benzonitrile. From the electrochemical analysis, the energies of the expected CS states are estimated to be lower than the triplet excited energies of the fullerene and porphyrin. $Li^+@C_{60}\subset H_4$–$CPD_{Py}(OC_6)$ undergoes photoinduced electron transfer from the triplet excited state of the porphyrin to $Li^+@C_{60}$ to afford the CS state. $Li^+@C_{60}\subset Ni_2$–$CPD_{Py}(OC_6)$ also undergoes photoinduced electron transfer from the nickel porphyrin to the triplet excited state of $Li^+@C_{60}$ with a rate constant of 5.7×10^7 s^{-1}. The lifetimes of the resulting CS states are 0.50 ms for $Li^+@C_{60}\subset H_4$–$CPD_{Py}(OC_6)$ and 0.67 ms for $Li^+@C_{60}\subset Ni_2$–$CPD_{Py}(OC_6)$. These CS lifetimes are the longest values ever reported for non-covalent porphyrin-fullerene supramolecules in solution and are attributed to the lower CS energies than the triplet energy of each chromophore.

Experimental section

Materials

Reagents and solvents of best grade available were purchased from commercial suppliers and were used without further purification unless otherwise noted. Lithium ion-encapsulated C_{60} ($Li^+@C_{60}$ PF_6^-: 96%) was obtained from Daiichi Jitsugyo Co. Ltd, Japan. *N*,*N*-Dimethylformamide (DMF) was purified by distillation from CaH_2 under reduced pressure. Benzonitrile (PhCN) was purified by distillation from P_2O_5 under reduced pressure after being stirred with K_2CO_3 overnight. Dry tetrahydrofuran (THF) was obtained by distillation from Na and benzophenone under N_2 atmosphere. Dry triethylamine (Et_3N) was obtained by distillation from CaH_2 under N_2 atmosphere, after being stirred with KOH overnight.

NMR and mass measurements

Nuclear magnetic resonance (NMR) spectra were recorded on a JEOL JNM-ECS400 (400 MHz for ^{1}H), JEOL JNM-ECA500 (500 MHz for ^{1}H), or Bruker AVANCE III 600 (151 MHz for ^{13}C) spectrometer. Chemical shifts were reported as δ values in ppm relative to tetramethylsilane. High-resolution fast atom bombardment mass spectra (HR-FAB-MS) were measured with 3-nitrobenzyl alcohol (NBA) as a matrix and recorded on a JEOL LMS-HX-110 spectrometer.

UV-vis and IR absorption measurements

Ultraviolet-visible (UV-vis) absorption and infrared (IR) spectra were recorded on Shimadzu UV-3100PC and BIO RAD FTS6000 spectrophotometers, respectively.

Emission measurements

Fluorescence spectra were measured on a Horiba FluoroMax-4 spectrofluorophotometer with a quartz cuvette (path length = 10 mm) at 298 K. Phosphorescence spectra were measured on a Horiba Fluorolog τ3 spectrophotometer with a quartz tube (i.d. = 4 mm) at 77 K.

Electrochemical measurements

Electrochemical measurements were performed on a ALS630B electrochemical analyzer in deaerated PhCN containing 0.1 M Bu_4NPF_6 as the supporting electrolyte at 298 K. A conventional three-electrode cell was used with a platinum working electrode (surface area of 0.3 mm^2) and a platinum wire as a counter electrode. The platinum working electrodes (BAS) were routinely polished with BAS polishing alumina suspension and rinsed with acetone and acetonitrile before use. The measured potentials were recorded with respect to an $Ag/AgNO_3$ (0.01 M) reference electrode. All potentials (*vs.* Ag/Ag^+) were converted to values *vs.* SCE by adding 0.29 V. All electrochemical measurements were carried out under an N_2 atmosphere.

Laser flash photolysis

Femtosecond transient absorption spectroscopy experiments were conducted using an ultrafast source: Integra-C (Quantronix Corp.), an optical parametric amplifier: TOPAS (Light Conversion Ltd) and a commercially available optical detection system: Helios provided by Ultrafast Systems LLC. The source for the pump and probe pulses were derived from the fundamental output of Integra-C (λ = 786 nm, 2 mJ per pulse and fwhm = 130 fs) at a repetition rate of 1 kHz. 75% of the fundamental output of the laser was introduced into a second harmonic generation (SHG) unit: Apollo (Ultrafast Systems) for excitation light generation at λ = 393 nm, while the rest of the output was used for white light generation. The laser pulse was focused on a sapphire plate of 3 mm thickness and then white

light continuum covering the visible region from $\lambda = 410$ nm to 800 nm was generated *via* self-phase modulation. A variable neutral density filter, an optical aperture, and a pair of polarizer were inserted in the path in order to generate stable white light continuum. Prior to generating the probe continuum, the laser pulse was fed to a delay line that provides an experimental time window of 3.2 ns with a maximum step resolution of 7 fs. In our experiments, a wavelength at $\lambda = 393$ nm of SHG output was irradiated at the sample cell with a spot size of 1 mm diameter where it was merged with the white probe pulse in a close angle (<10°). The probe beam after passing through the 2 mm sample cell was focused on a fiber optic cable that was connected to a CMOS spectrograph for recording the time-resolved spectra ($\lambda =$ 410–800 nm). Typically, 1500 excitation pulses were averaged for 3 seconds to obtain the transient spectrum at a set delay time. Kinetic traces at appropriate wavelengths were assembled from the time-resolved spectral data. All measurements were conducted at room temperature, 295 K.

Nanosecond time-resolved transient absorption measurements were carried out using the laser system provided by UNISOKU Co., Ltd. Measurements of nanosecond transient absorption spectrum were performed according to the following procedure. A deaerated solution containing supramolecule was excited by a Panther OPO pumped by a Nd:YAG laser (Continuum SLII-10, 4–6 ns fwhm). The photodynamics were monitored by continuous exposure to a xenon lamp (150 W) as a probe light and a photomultiplier tube (Hamamatsu 2949) as a detector. The solution was oxygenated by nitrogen purging for 15 min prior to measurements.

Synthesis

3-Bromo-5-(hexyloxy)benzaldehyde (1). 1,3-Dibromo-5-(hexyloxy)benzene[49] (3.36 g, 10 mmol) was added into a three-neck flask and the inside of the flask was replaced with N_2. Then, dry THF (100 mL) was added into the flask under N_2 atmosphere and the solution was cooled to −78 °C. To this solution, *n*-butyllithium (2.69 M solution in *n*-hexane, 3.7 mL, 10 mmol) was added dropwise over few minutes. An hour later, excess DMF was added to the reaction mixture. After warming to room temperature, the reaction was quenched with water. The reaction mixture was washed with water (100 mL, 2 times), dried over Na_2SO_4, and evaporated. The crude product was purified by column chromatography (silica-gel, *n*-hexane/$CHCl_3$ = 3/1 v/v) to furnish the product as a light yellow oil (2.64 g, 93 %). ^{1}H NMR ($CDCl_3$, 400 MHz): δ 0.91 (t, $J = 7.1$ Hz, 3H, –$(CH_2)_5CH_3$), 1.32–1.49 (m, 6H, –$(CH_2)_2(CH_2)_3CH_3$), 1.79 (quin, $J = 6.9$ Hz, 2H, –$CH_2CH_2(CH_2)_3CH_3$), 3.99 (t, $J = 6.6$ Hz, 2H, –$CH_2(CH_2)_4CH_3$), 7.30 (m, 2H, Ar–H), 7.55 (t, $J = 1.6$ Hz, 1H, Ar–H), 9.89 (s, 1H, –CHO); ^{13}C NMR ($CDCl_3$, 151 MHz): δ 14.1 (CH_3), 22.7 (CH_2), 25.7 (CH_2), 29.1 (CH_2), 31.6 (CH_2), 68.9 (OCH_2), 112.9 (aromatic C), 123.6 (aromatic C), 124.4 (aromatic C), 125.6 (aromatic C), 138.8 (aromatic C), 160.6 (aromatic C), 190.8 (CHO); HR-FAB-MS (NBA): *m*/*z* calcd for $C_{13}H_{18}O_2Br$: 285.0490; found: 285.0458; elemental analysis (%) calcd for $C_{13}H_{17}O_2Br$: C 54.75 H 6.01; found: C54.64 H 5.88.

3-Hexyloxy-5-(trimethylsilylethynyl)benzaldehyde (2). A solution of **1** (2.28 g, 8 mmol), palladium(II) acetate (18 mg, 80 μmol), and triphenyl phosphine (42 mg, 0.16 mmol) in dry Et_3N (8 mL) was degassed with a stream of N_2 for 30 min. Then, trimethylsilylacetylene (1.7 mL, 12 mmol) was added, heated rapidly to 80 °C, and stirred for 6 hours under N_2 atmosphere. After confirmation of the disappearance of Ar–H signals derived from the substrate, the reaction mixture was cooled to room temperature and the white precipitation was removed by filtration. The dark brown filtrate was evaporated and then purified by column chromatography (silica-gel, *n*-hexane/$CHCl_3$ = 3/1 v/v) to furnish the product as a thick brown oil (2.18 g, 90%). ^{1}H NMR ($CDCl_3$, 400 MHz): δ 0.26 (s, 9H, –$Si(CH_3)_3$), 0.91 (t, $J = 7.1$ Hz, 3H, –$(CH_2)_5CH_3$), 1.32–1.47 (m, 6H, –$(CH_2)_2(CH_2)_3CH_3$), 1.79 (quin, $J = 6.9$ Hz, 2H, –$CH_2CH_2(CH_2)_3CH_3$), 4.00 (t, $J = 6.4$ Hz, 2H, –$CH_2(CH_2)_4CH_3$), 7.23–7.24 (m, 1H, Ar–H), 7.33–7.34 (m, 1H, Ar–H), 7.53 (t, $J = 1.4$ Hz, 1H, Ar–H), 9.92 (s, 1H, –CHO); ^{13}C NMR ($CDCl_3$, 151 MHz): δ 0.0 ($SiCH_3$), 14.2 (CH_3), 22.7 (CH_2), 25.8 (CH_2), 29.2 (CH_2), 31.6 (CH_2), 68.7 (OCH_2), 95.9 (C≡C), 103.5 (C≡C), 113.9 (aromatic C), 124.3 (aromatic C), 125.3 (aromatic C), 126.9 (aromatic C), 137.8 (aromatic C), 159.6 (aromatic C), 191.6 (CHO); HR-FAB-MS (NBA): *m*/*z* calcd for $C_{18}H_{27}O_2Si$: 303.1780; found: 303.1789; elemental analysis (%) calcd for $C_{18}H_{26}O_2Si$: C 71.47 H 8.66; found: C 71.49 H 8.74.

5,15-Bis[3-hexyloxy-5-(trimethylsilylethynyl)phenyl]-10,20-di-[4-pyridyl]porphine (3). A solution of **2** (1.72 g, 5.7 mmol) and *meso*-(4-pyridyl)dipyrromethane[50] (1.27 g, 5.7 mmol) in 600 mL CH_2Cl_2 was degassed with a stream of N_2 for 30 min. To the resulting solution, trifluoroacetic acid (5.1 mL, 69 mmol) was added and stirred under N_2 atmosphere. After 30 min, 2,3-dichloro-5,6-dicyano-1,4-benzoquinone (1.94 g, 8.5 mmol) dissolved in THF was added and stirred for an hour. The reaction was finally quenched with Et_3N (10 mL, 72 mmol) and the mixture was purified by column chromatography (silica-gel, $CHCl_3$ then $CHCl_3$/THF = 40/1 v/v). The crude product was recrystallised from CH_2Cl_2/MeOH to give the product as a purple solid (475 mg, 17%). ^{1}H NMR ($CDCl_3$, 500 MHz): δ −2.92 (br-s, 2H, –NH), 0.26 (s, 18H, –$Si(CH_3)_3$), 0.90 (t, $J = 6.9$ Hz, 6H, –$(CH_2)_5CH_3$), 1.32–1.38 (m, 8H, –$(CH_2)_3(CH_2)_2CH_3$), 1.51 (quin, $J = 7.6$ Hz, 4H, –$(CH_2)_2CH_2(CH_2)_2CH_3$), 1.87 (quin, $J = 6.9$ Hz, 4H, –$CH_2CH_2(CH_2)_3CH_3$), 4.16 (t, $J = 6.5$ Hz, 4H, –$CH_2(CH_2)_4CH_3$), 7.44 (m, 2H, Ar–H), 7.71 (d, $J = 2.3$ Hz, 2H, Ar–H), 7.91 (d, $J = 7.9$ Hz, 2H, Ar–H), 8.16 (dd, $J = 1.5$ Hz, 2.3 Hz, 4H, Ar–H), 8.81 (d, $J = 4.6$ Hz, 4H, pyrrole *β*-H), 8.94 (d, $J = 4.6$ Hz, 4H, pyrrole *β*-H), 9.05 (d, $J = 6.1$ Hz, 4H, Ar–H); ^{13}C NMR ($CDCl_3$, 151 MHz): δ 0.1 ($SiCH_3$), 14.2 (CH_3), 22.7 (CH_2), 25.9 (CH_2), 29.4 (CH_2), 29.4 (CH_2), 31.7 (CH_2), 68.7 (OCH_2), 94.5 (C≡C), 105.1 (C≡C), 117.2 (aromatic), 117.3 (aromatic), 119.9 (aromatic C), 122.5 (aromatic C), 129.5 (aromatic C), 130.8 (aromatic C), 143.1 (aromatic C), 148.5 (aromatic C), 150.3 (aromatic C), 157.5 (aromatic C); HR-FAB-MS (NBA): *m*/*z* calcd for $C_{64}H_{68}N_6O_2Si_2$: 1008.4942; found: 1008.4897; elemental analysis (%) calcd for $C_{64}H_{68}N_6O_2Si_2$: C 76.15 H 6.79 N 8.33; found: C 76.05 H 6.80 N 8.12; UV-vis ($CHCl_3$): λ_{max} (ε, cm^{-1} M^{-1}) 420 (447800), 515 (19500), 549 (5700), 588 (5900), 646 (2700); IR (KBr): $\nu = 3318$, 2955, 2930, 2870, 2158, 1591, 1475, 1421, 1354, 1249, 1159, 976, 928, 855, 801, 760, 730, 660 cm^{-1}.

{5,15-Bis[3-hexyloxy-5-(trimethylsilylethynyl)-phenyl]-10,20-di[4-pyridyl]porphinato}zinc(II) (4). $Zn(OAc)_2 \cdot 2H_2O$ (0.90 g,

4.1 mmol) dissolved in MeOH was added to a solution of **3** (410 mg, 0.41 mmol) in 200 mL CH_2Cl_2. The resulting mixture was refluxed under N_2 atmosphere for 2 hours and cooled to room temperature. The reaction mixture was washed with water (200 mL, 2 times), dried over Na_2SO_4, and evaporated. The residue was purified by column chromatography (silica-gel, $CHCl_3$/EtOH = 100/1 v/v). The crude product was recrystallized from CH_2Cl_2/MeOH to give the product as a purple solid (0.41 g, 94 %). ^{1}H NMR (pyridine-d_5, 500 MHz): δ 0.32 (s, 18H, –Si(CH_3)$_3$), 0.79 (dd, J = 1.5 Hz, 5.4 Hz, 6H, –(CH_2)$_5$CH_3), 1.21–1.22 (m, 8H, –(CH_2)$_3$(CH_2)$_2$CH$_3$), 1.40–1.43 (m, 4H, –(CH_2)$_2$CH_2(CH_2)$_2$CH$_3$), 1.79 (quin, J = 7.1 Hz, 4H, –CH_2CH_2(CH_2)$_3$CH$_3$), 4.12 (t, J = 6.9 Hz, 4H, –CH_2(CH_2)$_4$CH$_3$), 7.81 (br-s, 2H, Ar–H), 8.13–8.15 (m, 2H, Ar–H), 8.32 (dd, J = 1.5 Hz, 2.3 Hz, 4H, Ar–H), 8.34 (d, J = 3.8 Hz, 2H, Ar–H), 9.07 (d, J = 4.6 Hz, 4H, pyrrole β-H), 9.18 (d, J = 6.0 Hz, 4H, Ar–H), 9.26 (d, J = 4.6 Hz, 4H, pyrrole β-H); ^{13}C NMR (pyridine-d_5, 151 MHz): δ 0.0 (SiCH_3), 14.2 (CH_3), 22.8 (CH_2), 26.0 (CH_2), 29.5 (CH_2), 31.7 (CH_2), 68.7 (OCH_2), 94.6 (C≡C), 106.3 (C≡C), 117.2 (aromatic C), 117.2 (aromatic C), 118.7 (aromatic C), 120.7 (aromatic C), 122.7 (aromatic C), 130.1 (aromatic C), 131.5 (aromatic C), 132.1 (aromatic C), 132.8 (aromatic C), 145.2 (aromatic C), 148.7 (aromatic C), 149.8 (aromatic C), 150.7 (aromatic C), 151.4 (aromatic C), 157.9 (aromatic C); HR-FAB-MS (NBA): m/z calcd for $C_{64}H_{66}N_6O_2Si_2Zn$: 1070.4077; found: 1070.4080; elemental analysis (%) calcd for $C_{64}H_{66}N_6O_2Si_2Zn \cdot 0.5CH_4O$: C 71.15 H 6.30 N 7.72; found: C 71.20 H 6.21 N 7.67; UV-vis ($CHCl_3$): λ_{max} (ε, cm^{-1} M^{-1}) 425 (455800), 554 (18000), 595 (3500); IR (KBr): ν = 2955, 2931, 2157, 1592, 1419, 1346, 1249, 1161, 1072, 998, 945, 855, 795, 760, 718, 667 cm^{-1}.

{5,15-Bis[3-ethynyl-5-(hexyloxy)phenyl]-10,20-di[4-pyridyl]porphinato}zinc(II) (5). A solution of **4** (111 mg, 0.1 mmol) and KF·2H_2O (68 mg, 0.72 mmol) in 5 mL of DMF/THF = 4/1 was stirred overnight under N_2 atmosphere. The reaction mixture was washed with H_2O (15 mL, 2 times), dried over Na_2SO_4, and evaporated. The crude product was recrystallized from $CHCl_3$/*i*-PrOH to give the product as a purple solid (92 mg, 96 %). ^{1}H NMR (pyridine-d_5, 500 MHz): δ 0.80 (t, J = 6.9 Hz, 6H, –(CH_2)$_5$CH_3), 1.22–1.23 (m, 8H, –(CH_2)$_3$(CH_2)$_2$CH$_3$), 1.44 (quin, J = 7.2 Hz, 4H, –(CH_2)$_2$CH_2(CH_2)$_2$CH$_3$), 1.81 (quin, J = 7.2 Hz, 4H, –CH_2CH_2-(CH_2)$_3$CH$_3$), 4.13 (t, J = 6.3 Hz, 4H, –CH_2(CH_2)$_4$CH$_3$), 4.28 (s, 2H, –C≡CH), 7.77 (br-s, 2H, Ar–H), 8.15 (d, J = 6.3 Hz, 2H, Ar–H), 8.30–8.33 (m, 6H, Ar–H), 9.10 (d, J = 4.6 Hz, 4H, pyrrole β-H), 9.18 (d, J = 5.2 Hz, 4H, Ar–H), 9.26 (d, J = 4.6 Hz, 4H, pyrrole β-H); ^{13}C NMR (pyridine-d_5, 151 MHz): δ 14.2 (CH_3), 22.8 (CH_2), 26.0 (CH_2), 29.6 (CH_2), 31.8 (CH_2), 68.7(OCH_2), 79.6 (C≡*C*H), 84.6 (*C*≡CH), 117.5 (aromatic C), 117.6 (aromatic C), 118.8 (aromatic C), 120.7 (aromatic C), 122.0 (aromatic C), 130.1 (aromatic C), 131.6 (aromatic C), 132.2 (aromatic C), 132.9 (aromatic C), 145.3 (aromatic C), 148.7 (aromatic C), 149.8 (aromatic C), 150.7 (aromatic C), 151.4 (aromatic C), 157.9 (aromatic C); HR-FAB-MS (NBA): m/z calcd for $C_{58}H_{50}N_6O_2Zn$: 926.3287; found: 926.3279; elemental analysis (%) calcd for $C_{58}H_{50}N_6O_2Zn \cdot 0.5CH_4O$: C 74.39 H 5.55 N 8.90; found: C 74.33 H 5.36 N 8.84; UV-vis ($CHCl_3$): λ_{max} (ε, cm^{-1} M^{-1}) 425 (463000), 553 (18300), 594 (3500); IR (KBr): ν = 2952, 2929, 2869, 1592, 1419, 1344, 1322, 1204, 1180, 1144, 1072, 998, 938, 795, 718, 676 cm^{-1}.

H_4–CPD$_{Py}$(OC$_6$). The free base dimer was prepared from **5** (186 mg, 0.2 mmol) according to the reported procedure.[35c] The crude product was purified by flash column chromatography (silica-gel, $CHCl_3$/EtOH = 200/1 v/v) and recrystallized from $CHCl_3$/*i*-PrOH to give the product as a purple solid (42 mg, 24 %). ^{1}H NMR ($CDCl_3$, 500 MHz): δ –3.04 (br-s, 4H, –NH), 0.94 (t, J = 6.9 Hz, 12H, –(CH_2)$_5$CH_3), 1.36–1.45 (m, 16H, –(CH_2)$_3$(CH_2)$_2$CH$_3$), 1.55–1.59 (m, 8H, –(CH_2)$_2$CH_2(CH_2)$_2$CH$_3$), 1.96 (quin, J = 6.9 Hz, 8H, –CH_2CH_2(CH_2)$_3$CH$_3$), 4.25 (t, J = 6.9 Hz, 8H, –CH_2(CH_2)$_4$-CH$_3$), 6.91 (s, 4H, Ar–H), 7.22 (s, 4H, Ar–H), 7.96 (br-s, 8H, Ar–H), 8.26 (s, 4H, Ar–H), 8.66 (d, J = 3.8 Hz, 8H, pyrrole β-H), 8.78 (d, J = 3.1 Hz, 8H, pyrrole β-H), 9.00 (br-s, 8H, Ar–H); ^{13}C NMR ($CDCl_3$, 151 MHz): δ 14.2 (CH_3), 22.8 (CH_2), 26.0 (CH_2), 29.5 (CH_2), 31.8 (CH_2), 68.9(OCH_2), 74.4 (C≡C), 83.2 (C≡C), 114.9 (aromatic C), 117.1 (aromatic C), 118.8 (aromatic C), 120.2 (aromatic C), 120.8 (aromatic C), 129.3 (aromatic C), 135.0 (aromatic C), 143.0 (aromatic C), 148.4 (aromatic C), 149.9 (aromatic C), 158.0 (aromatic C); HR-FAB-MS (NBA): m/z calcd for $C_{116}H_{100}N_{12}O_4$: 1724.7991; found: 1724.7997; elemental analysis (%) calcd for $C_{116}H_{100}N_{12}O_4 \cdot C_3H_8O$: C 80.01 H 6.09 N 9.41; found: C 80.12 H 5.90 N 9.44; UV-vis ($CHCl_3$): λ_{max} (ε, cm^{-1} M^{-1}) 419 (845300), 515 (36100), 549 (9200), 589 (10800), 646 (4300); IR (KBr): ν = 2953, 2928, 2869, 1590, 1475, 1417, 1370, 1195, 1171, 1056, 976, 799, 728, 660 cm^{-1}.

Ni$_2$–CPD$_{Py}$(OC$_6$). H_4–CPD$_{Py}$(OC$_6$) (29.5 mg, 17 μmol) and excess amount of Ni(OAc)$_2$·4H_2O dissolved in MeOH were refluxed in 17 mL $CHCl_3$/toluene (3/2) under N_2 atmosphere. After 5 days, the reaction mixture was washed with 1.0 M HCl, saturated aqueous solution of $NaHCO_3$, and water. The orange organic layer was dried over Na_2SO_4 and evaporated. The residue was purified by flash column chromatography (silica-gel, $CHCl_3$/EtOH = 250/1 v/v). The crude product was recrystallized from $CHCl_3$/*i*-PrOH to give the product as a orange solid (25.0 mg, 80 %). ^{1}H NMR ($CDCl_3$, 500 MHz): δ 0.94 (t, J = 6.9 Hz, 12H, –(CH_2)$_5$CH_3), 1.37–1.44 (m, 16H, –(CH_2)$_3$(CH_2)$_2$CH$_3$), 1.56–1.59 (m, 8H, –(CH_2)$_2$CH_2(CH_2)$_2$CH$_3$), 1.95 (quin, J = 7.1 Hz, 8H, –CH_2CH_2(CH_2)$_3$CH$_3$), 4.22 (t, J = 6.5 Hz, 8H, –CH_2(CH_2)$_4$CH$_3$), 6.60 (s, 4H, Ar–H), 7.21 (s, 4H, Ar–H), 7.81 (br-s, 8H, Ar–H), 8.19 (s, 4H, Ar–H), 8.56 (d, J = 4.6 Hz, 8H, pyrrole β-H), 8.68 (d, J = 5.4 Hz, 8H, pyrrole β-H), 8.88 (d, J = 5.4 Hz, 8H, Ar–H); ^{13}C NMR ($CDCl_3$, 151 MHz): δ 14.2 (CH_3), 22.8 (CH_2), 26.0 (CH_2), 29.4 (CH_2), 31.8 (CH_2), 68.9(OCH_2), 73.9 (C≡C), 81.8 (C≡C), 115.8 (aromatic C), 115.9 (aromatic C), 117.1 (aromatic C), 120.6 (aromatic C), 121.1 (aromatic C), 128.5 (aromatic C), 132.1 (aromatic C), 132.2 (aromatic C), 133.0 (aromatic C), 141.11 (aromatic C), 141.5 (aromatic C), 141.9 (aromatic C), 148.6 (aromatic C), 148.7 (aromatic C), 158.2 (aromatic C); HR-FAB-MS (NBA): m/z calcd for $C_{116}H_{96}N_{12}O_4Ni_2$: 1836.6384; found: 1836.6384; elemental analysis (%) calcd for $C_{116}H_{96}N_{12}O_4Ni_2 \cdot 0.5C_3H_8O$: C 75.48 H 5.39 N 8.99; found: C 75.30 H 5.11 N 9.02; UV-vis ($CHCl_3$): λ_{max} (ε, cm^{-1} M^{-1}) 415 (464000), 532 (30000); IR (KBr): ν = 2952, 2928, 2869, 1593, 1418, 1372, 1182, 1009, 796, 713, 671 cm^{-1}.

Acknowledgements

This work was supported by Grants-in-Aid (Scientific Research on Innovative Areas nos. 20108010 to S.F. and 20108009 to F.T.,

"pi-Space", 23750014 to K.O., and KOSEF/MEST through WCU project (R31-2008-000-10010-0), Korea. F.T. acknowledges Tokuyama Science Foundation and Iketani Science and Technology Foundation for Research Grants.

Notes and references

1 (*a*) A. J. Hoff and J. Deisenhofer, *Phys. Rep.*, 1997, **287**, 1; (*b*) *Anoxygenic Photosynthetic Bacteria*, ed. R. E. Blankenship, M. T. Madigan and C. E. Bauer, Kluwer Academic Publishers, Dordrecht, The Netherlands, 1995.

2 (*a*) D. Gust, T. A. Moore and A. L. Moore, *Acc. Chem. Res.*, 2001, **34**, 40; (*b*) G. Bottari, G. de la Torre, D. M. Guldi and T. Torres, *Chem. Rev.*, 2010, **110**, 6768; (*c*) D. Gust and T. A. Moore, in *The Porphyrin Handbook*, ed. K. M. Kadish, K. M. Smith and R. Guilard, Academic Press, San Diego, CA, 2000, vol. 8, p. 153; (*d*) D. Gust, T. A. Moore and A. L. Moore, in *Electron Transfer in Chemistry*, ed. V. Balzani, Wiley-VCH, Weinheim, 2001, vol. 3, p. 272.

3 (*a*) D. M. Guldi, G. M. A. Rahman, F. Zerbetto and M. Prato, *Acc. Chem. Res.*, 2005, **38**, 871; (*b*) D. Gust, T. A. Moore and A. L. Moore, *Acc. Chem. Res.*, 2009, **42**, 1890; (*c*) V. Sgobba and D. M. Guldi, *Chem. Soc. Rev.*, 2009, **38**, 165.

4 (*a*) M. R. Wasielewski, *Chem. Rev.*, 1992, **92**, 435; (*b*) M. R. Wasielewski, *Acc. Chem. Res.*, 2009, **42**, 1910.

5 (*a*) N. V. Tkachenko, L. Rantala, A. Y. Tauber, J. Helaja, P. H. Hynninen and H. Lemmetyinen, *J. Am. Chem. Soc.*, 1999, **121**, 9378; (*b*) M. Isosomppi, N. V. Tkachenko, A. Efimov and H. Lemmetyinen, *J. Phys. Chem. A*, 2005, **109**, 4881; (*c*) S. A. Vail, D. I. Schuster, D. M. Guldi, M. Isosomppi, N. Tkachenko, H. Lemmetyinen, A. Palkar, L. Echegoyen, X. Chen and J. Z. H. Zhang, *J. Phys. Chem. B*, 2006, **110**, 14155; (*d*) D. I. Schuster, K. Li, D. M. Guldi, A. Palkar, L. Echegoyen, C. Stanisky, R. J. Cross, M. Niemi, N. V. Tkachenko and H. Lemmetyinen, *J. Am. Chem. Soc.*, 2007, **129**, 15973.

6 J. L. Sessler, B. Wang, S. L. Springs and C. T. Brown, in *Comprehensive Supramolecular Chemistry*, ed. J. L. Atwood, J. E. D. Davies, D. D. MacNicol and F. Vögtle, Elsevier Science Ltd, Oxford, 1999, vol. 4, p. 311.

7 A. Osuka, N. Mataga and T. Okada, *Pure Appl. Chem.*, 1997, **69**, 797.

8 (*a*) K. D. Jordan and M. N. Paddon-Row, *Chem. Rev.*, 1992, **92**, 395; (*b*) M. N. Paddon-Row, *Acc. Chem. Res.*, 1994, **27**, 18.

9 M.-S. Choi, T. Yamazaki, I. Yamazaki and T. Aida, *Angew. Chem., Int. Ed.*, 2004, **43**, 150.

10 (*a*) S. Fukuzumi, *Org. Biomol. Chem.*, 2003, **1**, 609; (*b*) S. Fukuzumi, *Bull. Chem. Soc. Jpn.*, 2006, **79**, 177; (*c*) S. Fukuzumi, *Phys. Chem. Chem. Phys.*, 2008, **10**, 2283; (*d*) S. Fukuzumi and K. Ohkubo, *Coord. Chem. Rev.*, 2010, **254**, 372.

11 (*a*) S. Fukuzumi and K. Ohkubo, *J. Mater. Chem.*, 2012, **22**, 4575; (*b*) S. Fukuzumi, K. Ohkubo, F. D'Souza and J. L. Sessler, *Chem. Commun.*, 2012, **48**, 9801.

12 (*a*) K. Ohkubo and S. Fukuzumi, *J. Porphyrins Phthalocyanines*, 2008, **12**, 993; (*b*) K. Ohkubo and S. Fukuzumi, *Bull. Chem. Soc. Jpn.*, 2009, **82**, 303.

13 (*a*) S. Fukuzumi and T. Kojima, *J. Mater. Chem.*, 2008, **18**, 1427; (*b*) F. D'Souza and O. Ito, *Chem. Commun.*, 2009, 4913; (*c*) F. D'Souza and O. Ito, *Coord. Chem. Rev.*, 2005, **249**, 1410.

14 (*a*) S. Fukuzumi, K. Saito, K. Ohkubo, T. Khoury, Y. Kashiwagi, M. A. Absalom, S. Gadde, F. D'Souza, Y. Araki, O. Ito and M. J. Crossley, *Chem. Commun.*, 2011, **47**, 7980; (*b*) S. Fukuzumi, K. Ohkubo, K. Saito, Y. Kashiwagi and M. J. Crossley, *J. Porphyrins Phthalocyanines*, 2011, **15**, 1292.

15 S. Fukuzumi, I. Amasaki, K. Ohkubo, C. P. Gros, J.-M. Barbe and R. Guilard, *RSC Adv.*, 2012, **2**, 3741.

16 (*a*) T. Kojima, T. Honda, K. Ohkubo, M. Shiro, T. Kusukawa, T. Fukuda, N. Kobayashi and S. Fukuzumi, *Angew. Chem., Int. Ed.*, 2008, **47**, 6712; (*b*) S. Fukuzumi, T. Honda, K. Ohkubo and T. Kojima, *Dalton Trans.*, 2009, 3880; (*c*) T. Kojima, K. Hanabusa, K. Ohkubo, M. Shiro and S. Fukuzumi, *Chem.–Eur. J.*, 2010, **16**, 3646; (*d*) T. Honda, T. Nakanishi, K. Ohkubo, T. Kojima and S. Fukuzumi, *J. Am. Chem. Soc.*, 2010, **132**, 10155.

17 (*a*) F. D'Souza, E. Maligaspe, K. Ohkubo, M. E. Zandler, N. K. Subbaiyan and S. Fukuzumi, *J. Am. Chem. Soc.*, 2009, **131**, 8787; (*b*) F. D'Souza, N. K. Subbaiyan, Y. Xie, J. P. Hill, K. Ariga, K. Ohkubo and S. Fukuzumi, *J. Am. Chem. Soc.*, 2009, **131**, 16138; (*c*) F. D'Souza, A. N. Amin, M. E. El-Khouly, N. K. Subbaiyan, M. E. Zandler and S. Fukuzumi, *J. Am. Chem. Soc.*, 2012, **134**, 654; (*d*) F. D'Souza and O. Ito, *Chem. Soc. Rev.*, 2012, **41**, 86.

18 B. Grimm, J. Schornbaum, C. M. Cardona, J. D. van Paauwe, P. D. W. Boyd and D. M. Guldi, *Chem. Sci.*, 2011, **2**, 1530.

19 (*a*) S. Fukuzumi, *Pure Appl. Chem.*, 2007, **79**, 981; (*b*) S. Fukuzumi, in *Functional Organic Materials*, ed. T. J. J. Müller and U. H. F. Bunz, Wiley-VCH, 2007, pp. 465–510.

20 (*a*) L. Echegoyen, F. Diederich and L. E. Echegoyen, in *Fullerenes: Chemistry, Physics and Technology*, ed. K. M. Kadish and R. S. Ruoff, Wiley-Interscience, New York, 2000, pp. 1–51; (*b*) D. M. Guldi and S. Fukuzumi, in *Fullerenes: From Synthesis to Optoelectronic Properties*, ed. D. M. Guldi and N. Martin, Kluwer, Dordorecht, 2003, pp. 237–265.

21 (*a*) S. Fukuzumi and D. M. Guldi, in *Electron Transfer in Chemistry*, ed. V. Balzani, Wiley-VCH, Weinheim, 2001, vol. 2, pp. 270–337; (*b*) H. Imahori and S. Fukuzumi, *Adv. Funct. Mater.*, 2004, **14**, 525.

22 Y. Kashiwagi, K. Ohkubo, J. A. McDonald, I. M. Blake, M. J. Crossley, Y. Araki, O. Ito, H. Imahori and S. Fukuzumi, *Org. Lett.*, 2003, **5**, 2719.

23 K. Ohkubo, H. Imahori, J. Shao, Z. Ou, K. M. Kadish, Y. Chen, R. K. Pandey, M. Fujitsuka, O. Ito and S. Fukuzumi, *J. Phys. Chem. A*, 2002, **106**, 10991.

24 (*a*) K. Ohkubo, H. Kotani, J. Shao, Z. Ou, K. M. Kadish, G. Li, R. K. Pandey, M. Fujitsuka, O. Ito, H. Imahori and S. Fukuzumi, *Angew. Chem., Int. Ed.*, 2004, **43**, 853; (*b*) S. Fukuzumi, K. Ohkubo, H. Imahori, J. Shao, Z. Ou, G. Zheng, Y. Chen, R. K. Pandey, M. Fujitsuka, O. Ito and K. M. Kadish, *J. Am. Chem. Soc.*, 2001, **123**, 10676.

25 L. Matrín-Gomis, K. Ohkubo, F. Fernández-Lázaro, S. Fukuzumi and Á. Sastre-Santos, *J. Phys. Chem. C*, 2008, **112**, 17694.
26 F. D'Souza, R. Chita, K. Ohkubo, M. Tasior, N. K. Subbaiyan, M. E. Zandler, M. Rogacki, D. T. Gryko and S. Fukuzumi, *J. Am. Chem. Soc.*, 2008, **130**, 14263.
27 S. Fukuzumi, K. Ohkubo, H. Imahori and D. M. Guldi, *Chem.–Eur. J.*, 2003, **9**, 1585.
28 S. Fukuzumi, I. Nakanishi, T. Suenobu and K. M. Kadish, *J. Am. Chem. Soc.*, 1999, **121**, 3468.
29 P. V. Kamat, *J. Phys. Chem. C*, 2007, **111**, 2834.
30 A. Takai, M. Chkounda, A. Eggenspiller, C. P. Gros, M. Lachkar, J.-M. Barbe and S. Fukuzumi, *J. Am. Chem. Soc.*, 2010, **132**, 4477.
31 (*a*) P. D. W. Boyd and C. A. Reed, *Acc. Chem. Res.*, 2005, **38**, 235; (*b*) K. Tashiro and T. Aida, *Chem. Soc. Rev.*, 2007, **36**, 189; (*c*) D. Canevet, E. M. Pérez and N. Martín, *Angew. Chem., Int. Ed.*, 2011, **50**, 9248.
32 J.-M. Lehn, *Supramolecular Chemistry, Concepts and Perspectives*, VCH, Weinheim, 1995.
33 C. J. Chang, J. D. K. Brown, M. C. Y. Chang, E. A. Baker and D. G. Nocera, in *Electron Transfer in Chemistry*, ed. V. Balzani, Wiley-VCH, Weinheim, 2001, vol. 3, pp. 409–461.
34 (*a*) T. Hayashi and H. Ogoshi, *Chem. Soc. Rev.*, 1997, **26**, 355; (*b*) M.-J. Blanco, M. C. Jiménez, J.-C. Chambron, V. Heitz, M. Linke and J.-P. Sauvage, *Chem. Soc. Rev.*, 1999, **28**, 293; (*c*) I. Willner, E. Kaganer, E. Joselevich, H. Dürr, E. David, M. J. Günter and M. R. Johnston, *Coord. Chem. Rev.*, 1998, **171**, 261.
35 (*a*) H. Nobukuni, Y. Shimazaki, F. Tani and Y. Naruta, *Angew. Chem., Int. Ed.*, 2007, **46**, 8975; (*b*) H. Nobukuni, F. Tani, Y. Shimazaki, Y. Naruta, K. Ohkubo, T. Nakanishi, T. Kojima, S. Fukuzumi and S. Seki, *J. Phys. Chem. C*, 2009, **113**, 19694; (*c*) H. Nobukuni, Y. Shimazaki, H. Uno, Y. Naruta, K. Ohkubo, T. Kojima, S. Fukuzumi, S. Seki, H. Sakai, T. Hasobe and F. Tani, *Chem.–Eur. J.*, 2010, **16**, 11611.
36 (*a*) H. Nobukuni, T. Kamimura, H. Uno, Y. Shimazaki, Y. Naruta and F. Tani, *Bull. Chem. Soc. Jpn.*, 2012, **85**, 862; (*b*) H. Nobukuni, T. Kamimura, H. Uno, Y. Shimazaki, Y. Naruta and F. Tani, *Bull. Chem. Soc. Jpn.*, 2011, **84**, 1321.
37 (*a*) Y. Zeng, L. Biczok and H. Linchitz, *J. Phys. Chem.*, 1992, **96**, 5237; (*b*) D. M. Guldi and M. Maggini, *Gazz. Chim. Ital.*, 1997, **127**, 779; (*c*) D. M. Guldi, H. Hungerbuehler, I. Carmichael, K.-D. Asmus and M. Maggini, *J. Phys. Chem. A*, 2000, **104**, 8601.
38 (*a*) A. S. Aoyagi, E. Nishibori, H. Sawa, K. Sugimoto, M. Takata, Y. Miyata, R. Kitaura, H. Shinohara, H. Okada, T. Sakai, Y. Ono, K. Kawachi, K. Yokoo, S. Ono, K. Omote, Y. Kasama, S. Ishikawa, T. Komuro and H. Tobita, *Nat. Chem.*, 2010, **2**, 678; (*b*) S. Aoyagi, Y. Sado, E. Nishibori, H. Sawa, H. Okada, H. Tobita, Y. Kasama, R. Kitaura and H. Shinohara, *Angew. Chem., Int. Ed.*, 2012, **51**, 3377; (*c*) H. Okada, T. Komuro, T. Sakai, Y. Matsuo, Y. Ono, K. Omote, K. Yokoo, K. Kawachi, Y. Kasama, S. Ono, R. Hatakeyama, T. Kaneko and H. Tobita, *RSC Adv.*, 2012, **2**, 10624.
39 S. Fukuzumi, K. Ohkubo, Y. Kawashima, D. S. Kim, J. S. Park, A. Jana, V. Lynch, D. Kim and J. L. Sessler, *J. Am. Chem. Soc.*, 2011, **133**, 15938.
40 Y. Kawashima, K. Ohkubo and S. Fukuzumi, *J. Phys. Chem. A*, 2012, **116**, 8942.
41 K. Ohkubo, Y. Kawashima and S. Fukuzumi, *Chem. Commun.*, 2012, **48**, 4314.
42 Y. Matsuo, H. Okada, M. Maruyama, H. Sato, H. Tobita, Y. Ono, K. Omote, K. Kawachi and Y. Kasama, *Org. Lett.*, 2012, **14**, 3784.
43 Quasi-reversible CVs were observed in the electron oxidation processes because the adsorption on the electrode surface may occur due to the low solubility of the electrochemically oxidized porphyrin dimer.
44 L. X. Chen, X. Zhang, E. C. Wasinger, K. Attenkofer, G. Jennings, A. Z. Murean and J. S. Lindsey, *J. Am. Chem. Soc.*, 2007, **129**, 9616.
45 The formation dynamics of the CS state [H_4–$CPD_{Py}(OC_6)^{+}$+ $Li^{+}@C_{60}^{\cdot-}$]) could not be observed by the femto- and nanosecond laser flash photolysis because the process would occur in the 10 ns–100 ns time range, which is out of the range of the present laser flash systems.
46 In the case of the oligomeric porphyrin-fullerene systems, longer CS lifetimes (τ_{cs} = 0.70 and 0.84 ms) were observed due to the charge migration in the oligomeric arrays of the chromophores. See: S. Fukuzumi, K. Saito, K. Ohkubo, V. Troiani, H. Qiu, S. Gadde, F. D'Souza and N. Solladie, *Phys. Chem. Chem. Phys.*, 2011, **13**, 17019.
47 (*a*) R. A. Marcus and N. Sutin, *Biochim. Biophys. Acta, Rev. Bioenerg.*, 1985, **811**, 265; (*b*) R. A. Marcus, *Annu. Rev. Phys. Chem.*, 1964, **15**, 155.
48 The decay of $^{3}[Ni_2$–$CPD_{Py}(OC_6)]^{*}$ is much faster than electron transfer from $^{3}[Ni_2$–$CPD_{Py}(OC_6)]^{*}$ to $Li^{+}@C_{60}$. The rate of electron transfer from $^{3}[Ni_2$–$CPD_{Py}(OC_6)]^{*}$ to $Li^{+}@C_{60}$ is predicted as 10^{6}–10^{7} s^{-1} because the driving force of electron transfer ($-\Delta G_{ET}$ = 0.30 eV) is similar to the case of electron transfer from Ni_2–$CPD_{Py}(OC_6)$ to $^{3}[Li^{+}@C_{60}]^{*}$ ($-\Delta G_{ET}$ = 0.33 eV, $k_{ET} = 5.7 \times 10^{7}$ s^{-1}).
49 (*a*) Y. Zhang, C. Zhao, J. Yang, M. Kapiamba, O. Haze, L. J. Rothberg and M. -K. Ng, *J. Org. Chem.*, 2006, **71**, 9475; (*b*) W. Huang, M. Wang, C. Du, Y. Chen, R. Qin, L. Su, C. Zhang, Z. Liu, C. Li and Z. Bo, *Chem.–Eur. J.*, 2011, **17**, 440.
50 C. Ruzié, L. Michaudet and B. Boitrel, *Tetrahedron Lett.*, 2002, **43**, 7423.